PROCEEDINGS OF SCIENCE

Best Practices for the Manufacture of Antimatter Atoms

E. D. Hunter,[a,b,*] **M. Bumbar,**[a,b,c] **C. Amsler,**[d] **M. Bayo,**[e,f] **H. Breuker,**[g] **M. Cerwenka,**[c,d] **G. Costantini,**[h,i] **R. Ferragut,**[e,f] **M. Giammarchi,**[f] **A. Gligorova,**[d,1] **G. Gosta,**[h,i] **H. Higaki,**[j] **C. Killian,**[c,d] **V. Kraxberger,**[c,d] **N. Kuroda,**[k] **A. Lanz,**[c,d,2] **M. Leali,**[h,i] **G. Maero,**[f,l] **C. Malbrunot,**[a,3] **V. Mascagna,**[h,i] **Y. Matsuda,**[k] **S. Migliorati,**[h,i] **D. J. Murtagh,**[d] **A. Nanda,**[c,d] **L. Nowak,**[c,d] **M. Romé,**[f,l] **R. E. Sheldon,**[d] **M. C. Simon,**[d] **M. Tajima,**[b,m] **V. Toso,**[f,l] **S. Ulmer,**[g] **L. Venturelli,**[h,i] **A. Weiser,**[c,d] **E. Widmann**[d] **and Y. Yamazaki**[g]

[a] *Experimental Physics Department, CERN, Geneva, Switzerland*
[b] *Imperial College London, London, England*
[c] *Vienna Doctoral School in Physics, University of Vienna, Vienna, Austria*
[d] *Stefan Meyer Institute, Vienna, Austria*
[e] *Politecnico di Milano, Milan, Italy*
[f] *INFN sez. Milano, Milan, Italy*
[g] *Ulmer Fundamental Symmetries Laboratory, RIKEN Saitama, Japan*
[h] *Dipartimento di Ingegneria dell'Informazione, Università degli Studi di Brescia, Brescia, Italy*
[i] *INFN sez. Pavia, Pavia, Italy*
[j] *Graduate School of Advanced Science and Engineering, Hiroshima University, Hiroshima, Japan*
[k] *Insitute of Physics, the University of Tokyo, Komaba, Japan*
[l] *Dipartimento di Fisica, Università degli Studi di Milano, Milan, Italy*
[m] *Japan Synchrotron Radiation Research Institute, Hyogo, Japan*

E-mail: eric.david.hunter@cern.ch

We present a pulsed "e+kick" scheme for removing ions from a positron plasma, along with other plasma routines used by the ASACUSA-Cusp Collaboration for making antihydrogen in 2023 and 2024. We also report on selected antimatter mixing experiments from 2023. Antiprotons are introduced into a plasma of 4×10^6 positrons with variable RF heating and mixing speed. The effects of these variables on antihydrogen yield are interpreted in a way that is consistent with theoretical predictions. Our observations provide general guidance for stable antihydrogen production in Penning-Malmberg traps.

International Conference on Exotic Atoms and Related Topics and conference on Low Energy Antiprotons (EXA/LEAP 2024)
August 25-30, 2024
Vienna, Austria

[1] present address: University of Vienna, Vienna, Austria
[2] present address: University College London, London, England
[3] present address: TRIUMF, Vancouver, Canada
[*] Speaker

ISSN 1824-8039. Published by SISSA Medialab.

PoS(EXA-LEAP2024)021

1. Introduction

The CERN AD and ELENA facility [1–3] slows antiprotons ($\bar{p}$) to 100 keV, delivering bunches of 8–12 $\times$ 10^6 $\bar{p}$ in parallel to four different experiments every two minutes [4]. Most of these experiments use Penning-Malmberg traps [5] to make antihydrogen ($\bar{H}$) by combining $\bar{p}$ with positrons (e^+) (ALPHA [6], ASACUSA [7]) or positronium (AE$\bar{g}$IS [8], GBAR [9]). ALPHA traps $\bar{H}$ using a magnetic bottle, while the others seek to produce an $\bar{H}$ beam. All four groups devote weeks or months of beam time each year to improving control over the antimatter plasma in their traps. After decades of progress, much remains to be done, or even thought of. Meanwhile, certain ideas, such as the parallel energy analyzer [10], pulsed electron (e^-) kick-out [11], stacking [12], and SDREVC (simultaneous control of density and number of particles via the combination of compression and evaporative cooling) [13] are nowadays accepted as "standard best practice."

To this body of knowledge, we contribute some of our findings from experiments conducted in 2023 and 2024 in ASACUSA's MUSASHI [12] (Fig. 1) and Cusp trap [14]. In Section 2 we discuss plasma purification, $\bar{p}$ loss during recompression after stacking, and the effect of plasma temperature T on the measured space charge potential ϕ. In Section 3 we briefly explain three important factors in the conversion of $\bar{p}$ to $\bar{H}$ and present two experiments where one of the factors, T or $\bar{p}$ radius, is controlled by the independent variable. In Section 4 we list lessons learned.

2. Plasma Preparation

The plasma used for making $\bar{H}$ must be dense, pure (free from ions/e^- for e^+/$\bar{p}$ plasma), and as cold as possible. We begin with e^+ plasma purification, which limits the minimum achievable T when the number of particles $N \sim 10^6$ or more. We also consider trade-offs between plasma density n and $\bar{p}$ losses in the MUSASHI, where good compression is the key to effective transfer

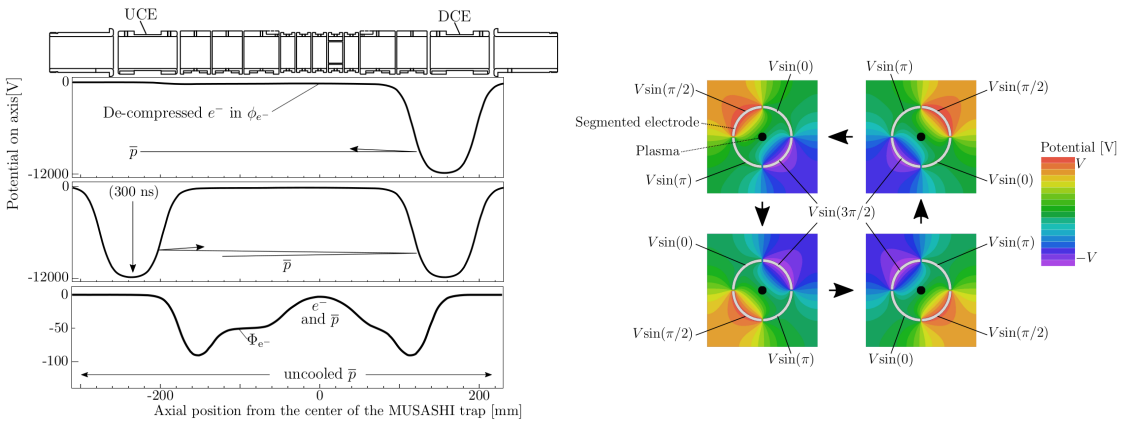

Figure 1: Cross section of the MUSASHI electrodes and potentials during $\bar{p}$ catching and cooling (left) and electric fields generated by periodic potentials applied to the azimuthally sectored rotating wall electrode (right). Antiprotons are cooled for at least 20 s before dropping the 12 kV barriers. Meanwhile, the rotating wall changes the rotation rate of the plasma and hence its density. After capture, the plasma must be compressed by the rotating wall to a radius 1 mm or less in order to escape the trap axially without clipping on focusing electrodes (downstream, not shown) in the transverse plane. Used with permission from Ref. [15]

to the Cusp trap. Achieving low T, high n, and high purity is only possible if we understand our trap and diagnostic systems, which are constantly evolving. We give one example at the end of this section: a cooling study with e^-, which we use to calibrate trap position and our ϕ diagnostic.

2.1 Positrons

Most antimatter traps are open on at least one side. Gas puffs from gate valves, hot filaments of gauges and e^- emitters, or simply room temperature surfaces, all breathe a wind of neutral gas molecules into the trap. We estimate that a typical room temperature molecule passing through a 5 cm long positron plasma with $n = 10^8\,\mathrm{cm}^{-3}$ and $kT \sim 5\,\mathrm{eV}$ has about 1 chance in 10^4 of being ionized (for relevant cross sections, see Ref. [16]). Such a high temperature is possible at the start of rotating wall compression [17] or when the voltage of an electrode is pulsed in a time $t \leq 1/\omega_z$, where ω_z is 2π times the axial bounce frequency [18]. The resulting ions may become trapped, contaminating the plasma. Collisions of unlike species in the radial electric field of the plasma cause cross field (mobility) transport. The ensuing plasma expansion raises T because transport down the field gradient turns electric potential energy into kinetic energy. Minimizing T requires ion removal.

In Fig. 2 we illustrate two methods for removing ions from a e^+ plasma. Ion heating, Fig. 2(a), causes ions to leave the plasma axially (or radially) by sweeping the frequency of an oscillating field through the ion bounce (or cyclotron) frequency (typically 400 sweeps, 10–1000 kHz, 20 ms duration). e+kick, Fig. 2(b), purifies the e^+ by passing them from one well to another too quickly for the ions to follow. While Fig. 2(a) may look simpler, ion heating is actually less robust than e+kick because the sweep parameters and well shape have to be tuned for each value of n, N, and ion load, which we can't exactly control prior to ion removal. In practice, ion heating takes much longer to optimize, and it is not clear if it works at all for large values of N. The routine seems to require more and more sweeps as N increases, yet we observe diminishing returns past 400 sweeps.

We compare the results of the two methods in Fig. 3. Both methods reduce T by removing ions. Neither one achieves 100% purity. For $N > 10^7$, T seems to be stuck about 10 K above the T measured for an equivalent electron plasma. The data also suggests that ion heating yields fewer ions in the final state than e+kick. Unfortunately, we cannot perform a fair comparison here. The Cusp Exit Gate Valve was open only for the e+kick tests, not the ion heating tests. With the gate valve open, we observe a higher $\bar{p}$ annihilation rate, higher $\bar{p}$ temperature, and reduced purity of both $\bar{p}$ and e^+ plasma. We left it open for the e+kick tests for consistency with $\bar{H}$ production runs, where it must be open so that $\bar{H}$ can leave the trap. The ion heating scans were done months before the 2024 $\bar{H}$ campaign, so it did not occur to us to open the gate valve for those.

To estimate the number of ions, we first measure the microchannel plate gain with e^- (5.3 V for $11 \times 10^3\,e^-$) using the same front-back bias on the microchannel plate as for ions (900 V). We divide the ion signal by the gain times the ratio of detection efficiency for ions of hydrogen (5–15% at 180 eV [19]) and e^- (50–70% at 170 eV [20]). This crude approximation gives $0.5\text{–}2.5 \times 10^3$ for the number of ions remaining after e+kick, implying that the purity exceeds 99.99% for the $N = 130 \times 10^6\,e^+$ plasma.

The bottom line is, e+kick is easier to develop and gives more consistent results. Mainly one needs a deep enough well, a low pulse amplitude (to avoid generating more ions), and a long time between pulses so that the core is replenished (see end of Section 3). These parameters are fixed

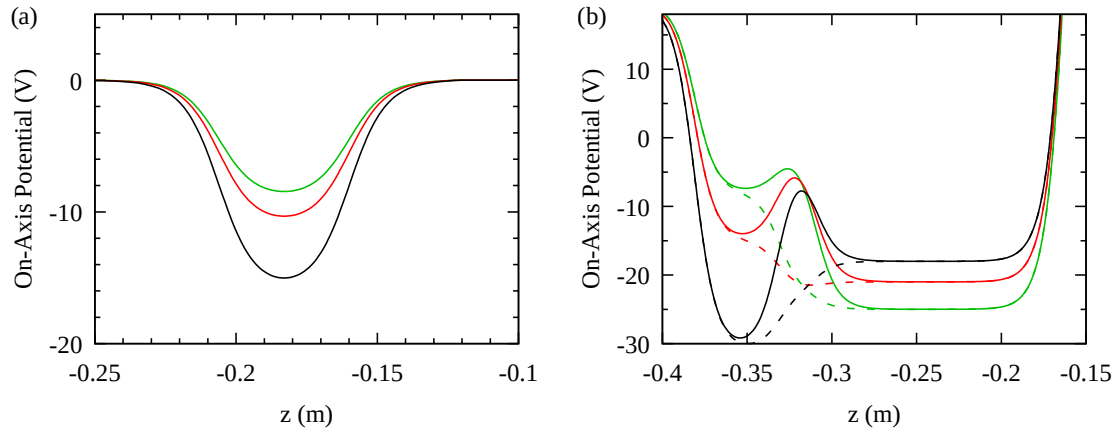

Figure 2: Trapping potential vs. axial position z for two ion removal methods. (a) Ion heating: well depth is tuned such that the plasma is poorly confined, so that particles with a little extra energy can escape. RF swept through the ion bounce frequencies preferentially adds energy to the ions. Optimal heating wells are shown for $N = 10,\ 20,\ 37 \times 10^6\ e^+$ (green, red, black). (b) e+kick: the plasma is held initially at $z = -0.36$ m. The barrier at $z = -0.32$ m is pulsed down for 50 ns (solid $\rightarrow$ dashed potentials), long enough for most of the e^+ to reach the right side, and short enough that few ions do. This is done first in the black well, then in progressively shallower wells as ϕ shifts from left to right.

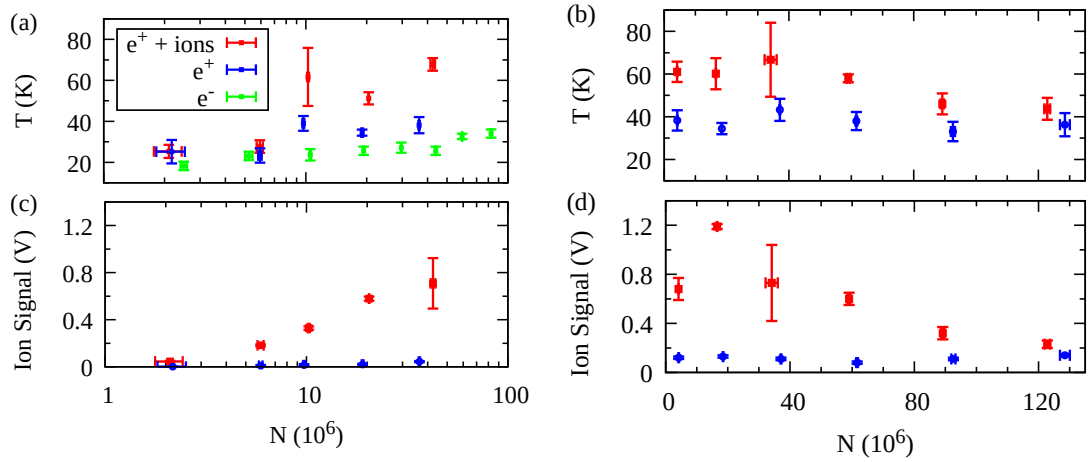

Figure 3: Effect of ion removal on e^+ T and comparison to e^- T. T and ion signal are shown (a,c) with and without ion heating and (b,d) with and without e+kick. Key to (a) shows color code for (a-d).

for all values of N in Fig. 3. Ion heating, in contrast, requires one to tune several parameters on a per-N basis. The well must be as shallow as possible, to minimize the ion temperature needed for ions to escape. The e^+ must be heated enough to reduce collisional cooling of the ions, but not so much that they breed more ions. The RF must sweep through ion resonances but no plasma modes. Optimal tuning depends on N and initial ion load, which can vary from day to day.

2.2 Antiprotons

The MUSASHI is good at capturing $\bar{p}$—best in the world for over a decade [11]—but it is challenging to get them back out. Using a pulsed drift tube to optimize the incoming beam energy, we trap and cool over 25% of the $\bar{p}$ delivered by ELENA [21]. For one stack of $\bar{p}$ from the AD, we obtain nearly 80% transfer efficiency, meaning most of the losses are at the 79% transparent copper mesh covering the entrance to the Cusp trap [22]. For three stacks (three consecutive bunches from the AD, spaced two minutes apart), the transfer efficiency is lower. Three stacks only gives 70% more $\bar{p}$ in the Cusp than one stack, with more $\bar{p}$ annihilation at transfer. Those $\bar{p}$ are "skimmed-off" as they leave the stronger field of the trap (the radial coordinate increases as the magnetic field decreases). They are a symptom of insufficient plasma compression.

We notice a trade-off between good compression and $\bar{p}$ annihilation. Turning on the rotating wall [17] causes some of the $\bar{p}$ to annihilate, especially after the plasma has had time to expand. Curiously, it seems that more $\bar{p}$ annihilate on the trap wall when the frequency of the rotating wall is correctly tuned such that the rest of the $\bar{p}$ are compressed (higher transfer efficiency). Perhaps centrifugal separation [23, 24] puts some $\bar{p}$ at high radius, where there are too few e^- for effective cooling, or perhaps the $\bar{p}$ are at such high radius that the rotating wall field is anharmonic and drives the plasma off axis. Our experiments seem to contradict those hypotheses. One may also consider the "electron tails" hypothesis proposed by Krasnicky et al. [25], which we cannot verify in our system because of limited dynamic range of the detector downstream of the MUSASHI.

So far, best results obtain when the plasma is held in a single well with the rotating wall fixed at 600 kHz and 4 V for the entire six-minute stacking procedure, then recompressed before transfer. This keeps the $\bar{p}$ from drifting to higher radius. Better results may be possible. Constant compression between stacks is not ideal, since we want e^- to cover as much area as possible when the bunch arrives from the AD. Otherwise the capture efficiency becomes sensitive to small changes in beam steering induced by activities from other groups in the hall, such as magnet ramping and use of the overhead crane.

2.3 Electrons

The emission of cyclotron radiation from e^- and e^+ cools the plasma [26]. In free space, T approaches equilibrium with the radiation field at a rate $\Gamma_0 \approx 0.26\,\mathrm{s}^{-1} \times B^2$, where B is the magnetic field in tesla. In the Cusp trap, we can measure Γ by heating the plasma to a known temperature $T_0 = 10000\,\mathrm{K}$, cooling for a variable time, and diagnosing T. The result of such a scan is shown in Fig. 4(a). We repeat the scan, cooling the plasma at different axial locations z, to obtain a map $\Gamma(z)$. In Fig. 4(b) we compare $\Gamma(z)$ to $\Gamma_0(z)$ using a simulated map $B(z)$ provided by JASTEC (checked at CERN by sliding a Hirst GM-05 Hall probe through the center of the Cusp magnet bore). We take the square root of the ordinates and minimize χ^2 for variable offset Δz applied to $\Gamma_0(z)$. The best fit value $\Delta z = 3.5 \pm 4.5\,\mathrm{mm}$, where the error bars come from letting χ^2 increase by 25%. This suggests that the trap electrodes are within a few millimeters of their nominal position in the magnet.

The parallel energy analyzer [10] diagnoses both T and ϕ. The (exponential) slope of the red curve in Fig. 5(a) is $\frac{e}{k_B T}$, where e is the elementary charge and k_B is Boltzmann's constant. The curve's left endpoint, where it reaches the noise floor, is an estimate of ϕ. Figure 5(b) shows how

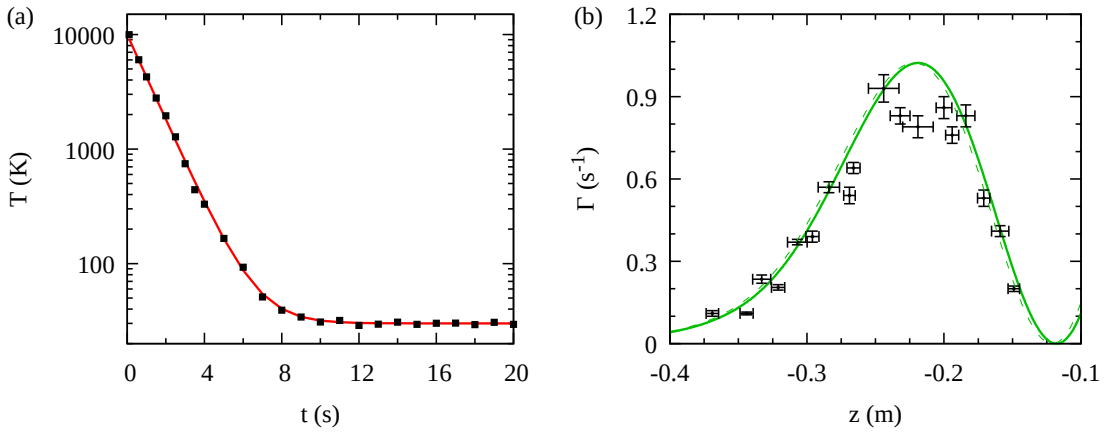

Figure 4: Electron cooling measurements. (a) Cooling curve at $z = -0.200$ m. The red fit uses $T_0 = 10000$ K, $T_f = 30$ K, and $\Gamma = 0.86\,\mathrm{s}^{-1}$. (b) Cooling rate as a function of z. The theory curve (dashed green line) is offset by 3 mm (solid green line) with respect to the nominal trap position. The discrepancy for $\Gamma > 0.8\,\mathrm{s}^{-1}$ could be a cavity effect. In a trap, Γ can be enhanced or suppressed by cavity modes, which concentrate radiation power at special frequencies and trap locations [26, 27].

this estimate depends on T, for the aggregated data of Fig. 4. Since every plasma used for that dataset had the same length, radius, and N, ϕ should be the same for all, independent of cooling time etc. We observe an error $\Delta\phi \approx 10\frac{k_B T}{e}$ which is equivalent to the following statement: the signal in Fig. 5(a) rises above the background when at least $180\,e^-$ are released per $\frac{k_B T}{e}$ of change in confinement potential. The number 180 is $N = 1.2 \times 10^7$ times the integral of a Boltzmann distribution over the energy range 9.5–10.5$k_B T$. The number required may depend on detector sensitivity. For a 100% efficient plasma particle detector, we expect a straight line, probably with a steeper slope than the one in Fig. 5(b). The nonlinearity for $T > 0.5$ eV suggests that this is where events are spread too thin in time for pileup to boost the signal above the noise. This reasoning also lets us estimate the signal-to-noise ratio. The confinement is ramped at 3.8 V/ms, so at $T \approx 0.5$ eV there are $180 * 3.8/0.5/1000 = 1.4\,e^-$ per 1 μs, which is the RC time constant of our SiPM detector. In other words, roughly $2\,e^-$ must arrive simultaneously to be distinguished from the noise.

3. Mixing Experiments

A slow $\bar{p}$ inside a cold, dense e^+ plasma can capture a e^+ and form $\bar{H}$ via three-body recombination, $\bar{p} + e^+ + e^+ \rightarrow \bar{H} + e^+$ [28, 29]. The $\bar{H}$ is weakly bound and will break up when it reaches the edge of the plasma [30] unless the binding energy, initially of order $k_B T$, increases via collisions with e^+ in the plasma [31]. More often, the atom is instead ionized by these collisions. This cycle ($\bar{p} \rightarrow \bar{H} \rightarrow \bar{p}$) repeats until the $\bar{p}$ leaves the plasma axially, gets stuck at the radial edge, or succeeds (many consecutive "lucky" collisions) in binding a e^+ strongly enough ($5k_B T$ [32, 33]) to survive further collisions and edge fields. The e^+ plasma properties n and T determine the collision rate, hence how many chances the $\bar{p}$ has to form strongly bound $\bar{H}$. Lower T always increases the amount of stable $\bar{H}$. In most cases, lower T also increases the average binding energy, because the smaller step size ($k_B T$ per collision) is outweighed by the greater number of collisions. In contrast, it is not

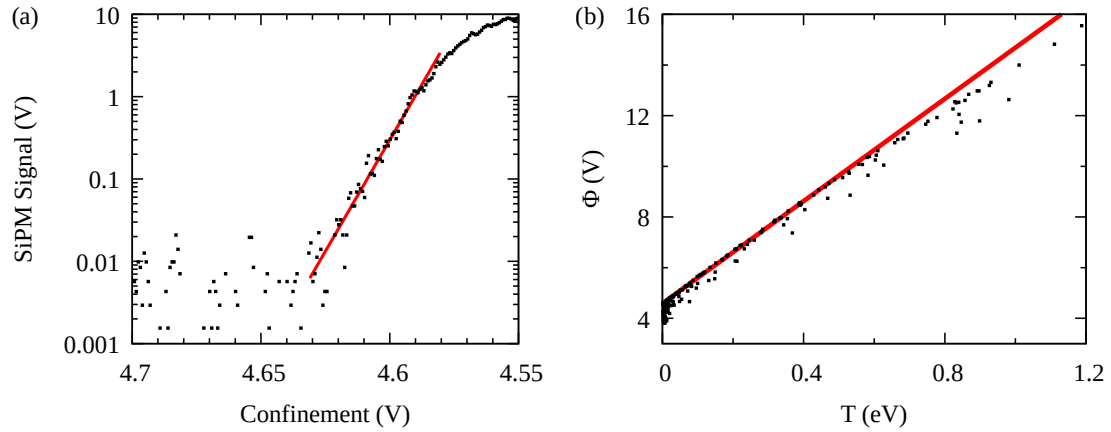

Figure 5: Diagnosis of T and ϕ. (a) A single trace, with fit values $T = 93$ K and $\phi = 4.631$ V. (b) Estimated ϕ as a function of T for all traces used in Fig. 4. Data points are black and trend lines are red.

Species	N (10^6)	ϕ (V)	T (K)	R (mm)	n (cm^{-3})
e^+	4.0	1.6	25	0.4	1.6×10^8
$\bar{p}$	>0.3	0.4	100	0.8	2.0×10^7

Table 1: Plasma properties before mixing: number of particles (N), space charge (ϕ), temperature (T), average radius (R), and density (n) assuming a uniform cylinder of charge. For the $\bar{p}$, N was only measured once, by slowly releasing $\bar{p}$ (over one hour, because of DAQ limitations) to a single-particle detector. 3.5×10^5 events passed the threshold, of which at most 1% could be background (or e^-). 3×10^5 is a reasonable lower bound for N given the cycle-to-cycle consistency of total AMT counts. This estimate ignores the mesh between trap and detector.

useful to increase n beyond 10^8–10^9 cm^{-3} because it raises the radial electric field, which imparts additional transverse momentum to the $\bar{p}$.

We present two $\bar{H}$ experiments, one with variable RF heating power and one with variable mixing speed. Higher heating power increases T. Faster mixing increases the average radius at which $\bar{p}$ enter the e^+ plasma. By the foregoing discussion, both reduce the chances of making stable $\bar{H}$, which we diagnose via the relative $\bar{H}$ yield

$$Y = \frac{\text{counts during mixing}}{\text{total counts}} \tag{1}$$

where "counts" refers to 2- or 3-fold coincident discriminated photomultiplier signals from the 7-panel scintillator of the ASACUSA Micromegas Tracker (AMT) [34]. We conclude each mixing experiment by dumping any uncombined $\bar{p}$ to the Cusp's first field null, directly under the AMT. The plasma properties at the start of mixing are listed in Table 1.

Equation 1 neglects the difference in 2- and 3-coin counting efficiency for annihilations in the mixing region vs. those at the null dump, which happen closer to the center of the AMT. This causes us to underestimate Y. The underestimate should be minor when Y is large, but could be significant when Y is small. Annihilation of e^+ during mixing could also bias Y. The per-channel detection

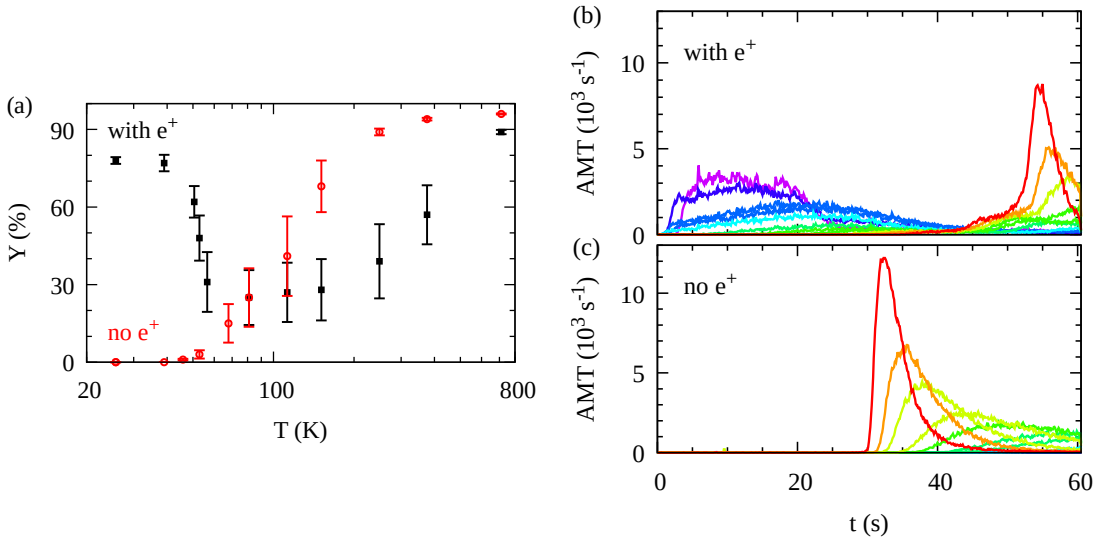

Figure 6: Annihilation fraction during mixing and annihilation rate vs. RF heating power. (a) "Y" (here, annihilation fraction is not necessarily $\bar{H}$ fraction) given as the average of 2- and 3- coincidence ratios, for variable noise power P. Error bars are the difference between 2-coin and 3-coin ratios. The x-axis is converted from P to e^+ $T = T_0 + mP$, where $T_0 = 25\,\mathrm{K}$ and $m = 70\,\mathrm{K/mW}$. (b) Annihilation rate recorded by the AMT scintillator. Line color (purple, blue, green, orange, red) goes from lowest to highest heating power (25–711 mW into 50 Ω).

efficiency is 100× lower for e^+ than for $\bar{p}$, so that factor could artificially increase Y by about 1%. Thus, graphs of Y should be considered qualitative.

3.1 RF Heating

To change T, we apply white noise to the electrode farthest from the $\bar{p}$ [35]. Unlike in Ref. [36], which uses resonant heating, here the heating rate does not depend strongly on properties of the e^+ plasma [37]. However, white noise heats both e^+ and $\bar{p}$. To better distinguish the effects of e^+ and $\bar{p}$ heating, we (i) repeat the test with no e^+ and (ii) interrupt mixing at $t = 10\,\mathrm{s}$ (1/6 of the way through the cycle) to measure e^+ T. The latter gives us a linear scale for converting noise power to e^+ T. The results are shown in Fig. 6.

Raising the heating power increases T and reduces Y. Y drops sharply (T^{-x} with $2 \lesssim x \lesssim 3$) in the range $50 < T < 60\,\mathrm{K}$. If we speculate that it is not possible to convert more than 80% of the $\bar{p}$ in this system, for instance due to incomplete spatial overlap of the plasma, then all T below some value (here, about 50 K) should give the same $Y = 80\%$. For higher heating power, the annihilation signal increases, with or without e^+ in the trap. We think that those annihilations are $\bar{p}$ that escape the trapping potential axially. Position reconstruction using an array detector [38] shows that they occur far upstream of the mixing region. The AMT count rate, Fig. 6(b,c), also shows an exponential increase in time for high heating power. Those non-$\bar{H}$ annihilations begin at slightly lower noise power for the case of no e^+, and are more intense in that case, implying that the e^+ protect the $\bar{p}$ somewhat, either by reducing the amplitude of the noise electric field or by collisionally cooling them.

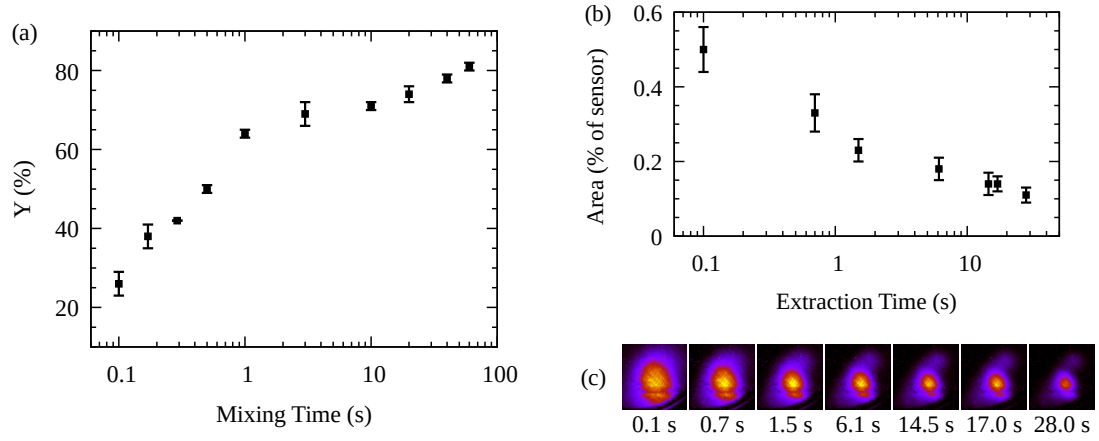

Figure 7: Mixing at variable voltage ramp rate. (a) Y vs. mixing time. Average and error bars same as Fig. 6. (b,c) Images of a slowly extracted $\bar{p}$ beam and beam area expressed as the fraction of camera pixels above threshold, where the threshold is set to $1/4$ times the peak intensity for each image. The z-scale maximum for each image is proportional to the beam area. The minimum is the same for all images. Error bars give standard deviation in the area when the threshold is varied by ±25%. (This area-based method is more reliable than 2D Gaussian fits, which can fail due to distortion in the larger-radius images.)

The on-axis potential is modified by ϕ. For the heating data without e^+, we apply a vacuum potential that mimics the effect of the e^+ ϕ, that is, we make the middle of the nested well flatter and shallower. This allows $\bar{p}$ to cross over the middle earlier in the cycle. If we don't modify the potential, we see no $\bar{p}$ annihilations for at least $2/3$ of the cycle, for the full range of noise power. This shows that the noise only heats the $\bar{p}$ that pass through the e^+ (or over the mimic potential if no e^+) and reach the other side of the nested well, where the noise power density is greater.

3.2 Mixing Speed

Figure 7(a) shows how Y increases when the $\bar{p}$ are pushed into the e^+ more slowly. Mixing, like slow extraction [39], preferentially removes particles close to the trap axis. The $\bar{p}$ and e^+ plasma need time to fill back in, or else the plasma is hollow and $\bar{H}$ is formed at higher radius. We make a connection between mixing and slow extraction in Fig. 7(b,c), where the same $\bar{p}$ plasma is slowly released to an imaging detector (instead of mixing) with variable ramp time. The time dependence of Y in (a) is similar to the time dependence of the extraction radius in (b).

Mixing, slow extraction, evaporative cooling, and the parallel energy analyzer all depend on how the core of the plasma is refilled as particles escape. The limiting time scale must be set by the finite length diocotron instability growth rate [40, 41] of the species with smaller N/L, where L is the plasma length. We are not aware of any explicit study of this process in the literature (the hollow beam in Ref. [39] is produced by a trajectory simulation). Its relation to Y has not been explored in previous experiments, which either lacked sufficient plasma diagnostics [42, 43] or relied on temporary cooling methods (such as adiabatic expansion) that make it difficult to study long-timescale effects [44].

4. Conclusion

We summarize our findings as a list of suggestions. The reader who follows them is likely to improve plasma control and increase stable $\bar{H}$ production in their experiment.

1. Purify e^+ using e+kick.
2. Keep $\bar{p}$ close to the trap axis.
3. To get the best estimate of ϕ, scan T and extrapolate to $T = 0$.
4. Cool e^+ to 40 K or less.
5. Mix as slowly as possible.

Acknowledgments

This work is supported by CERN; DFG (Germany); FWF P 32468 and W1252-N27 (Austria); INFN (Italy); JSPS KAKANHI 19KK0075, 20H01930, and 20KK0305 (Japan); RIKEN (Japan); and the Royal Society (UK).

References

[1] S. Maury, *The Antiproton Decelerator: AD*, *Hyperfine Interactions* **109** (1997) 43.

[2] S. Maury, W. Oelert, W. Bartmann, P. Belochitskii, H. Breuker, F. Butin et al., *ELENA: The extra low energy anti-proton facility at CERN*, *Hyperfine Interactions* **229** (2014) 105.

[3] C. Carli, D. Gamba, C. Malbrunot, L. Ponce and S. Ulmer, *ELENA: bright perspectives for low energy antiproton physics*, *Nuclear Physics News* **32** (2022) 21.

[4] L. Bojtar, Y. Dutheil, B. Lefort, D. Gamba, B. Dupuy, P. Freyermuth et al., *JACoW: A review of the 2023 antiproton physics run in the CERN antimatter factory*, *JACoW IPAC* **2024** (2024) TUPC08.

[5] J. H. Malmberg and C. F. Driscoll, *Long-time containment of a pure electron plasma*, *Physical Review Letters* **44** (1980) 654.

[6] G. Andresen, W. Bertsche, A. Boston, P. D. Bowe, C. Cesar, S. Chapman et al., *Production of antihydrogen at reduced magnetic field for anti-atom trapping*, *Journal of Physics B: Atomic, Molecular and Optical Physics* **41** (2007) 011001.

[7] Y. Enomoto, N. Kuroda, K. Michishio, C. H. Kim, H. Higaki, Y. Nagata et al., *Synthesis of cold antihydrogen in a cusp trap*, *Physical Review Letters* **105** (2010) 243401.

[8] C. Amsler, M. Antonello, A. Belov, G. Bonomi, R. S. Brusa, M. Caccia et al., *Pulsed production of antihydrogen*, *Communications Physics* **4** (2021) 19.

[9] P. Adrich, P. Blumer, G. Caratsch, M. Chung, P. Cladé, P. Comini et al., *Production of antihydrogen atoms by 6 keV antiprotons through a positronium cloud*, *The European Physical Journal C* **83** (2023) 1004.

[10] D. L. Eggleston, C. F. Driscoll, B. R. Beck, A. W. Hyatt and J. H. Malmberg, *Parallel energy analyzer for pure electron plasma devices*, *Physics of Fluids B: Plasma Physics* **4** (1992) 3432.

[11] N. Kuroda, H. A. Torii, K. Y. Franzen, Z. Wang, S. Yoneda, M. Inoue et al., *Confinement of a large number of antiprotons and production of an ultraslow antiproton beam*, *Physical Review Letters* **94** (2005) 023401.

[12] N. Kuroda, H. A. Torii, Y. Nagata, M. Shibata, Y. Enomoto, H. Imao et al., *Development of a monoenergetic ultraslow antiproton beam source for high-precision investigation*, *Physical Review Special Topics - Accelerators and Beams* **15** (2012) 024702.

[13] M. Ahmadi, B. X. R. Alves, C. J. Baker, W. Bertsche, A. Capra, C. Carruth et al., *Enhanced control and reproducibility of non-neutral plasmas*, *Physical Review Letters* **120** (2018) 025001.

[14] N. Kuroda, M. Tajima, B. Radics, P. Dupré, Y. Nagata, C. Kaga et al., *Antihydrogen synthesis in a double-cusp trap*, *Proceedings of the 12th International Conference on Low Energy Antiproton Physics (LEAP2016)* (2017) 011009.

[15] M. Tajima, *Development of injection scheme of antiprotons and production of antihydrogen atoms in low-lying excited states*, Ph.D. thesis, University of Tokyo, 2017.

[16] J. Marler and C. Surko, *Positron-impact ionization, positronium formation, and electronic excitation cross sections for diatomic molecules*, *Physical Review A—Atomic, Molecular, and Optical Physics* **72** (2005) 062713.

[17] J. R. Danielson, C. M. Surko and T. M. O'Neil, *High-density fixed point for radially compressed single-component plasmas*, *Physical Review Letters* **99** (2007) 135005.

[18] B. Cluggish, J. Danielson and C. Driscoll, *Resonant particle heating of an electron plasma by oscillating sheaths*, *Physical Review Letters* **81** (1998) 353.

[19] B. Peko and T. Stephen, *Absolute detection efficiencies of low energy h, h-, h+, h2+ and h3+ incident on a multichannel plate detector*, *Nuclear Instruments and Methods in Physics Research Section B: Beam Interactions with Materials and Atoms* **171** (2000) 597.

[20] G. Fraser, *The electron detection efficiency of microchannel plates*, *Nuclear Instruments and Methods in Physics Research* **206** (1983) 445.

[21] C. Amsler, H. Breuker, M. Bumbar, S. Chesnevskaya, G. Costantini, R. Ferragut et al., *Injection and capture of antiprotons in a Penning-Malmberg trap using a drift tube accelerator and degrader foil*, *Nuclear Instruments and Methods in Physics Research Section A: Accelerators, Spectrometers, Detectors and Associated Equipment* (2024) 169529.

[22] C. Amsler, H. Breuker, S. Chesnevskaya, G. Costantini, R. Ferragut, M. Giammarchi et al., *Reducing the background temperature for cyclotron cooling in a cryogenic Penning–Malmberg trap*, *Physics of Plasmas* **29** (2022) 083303.

[23] T. O'Neil, *Centrifugal separation of a multispecies pure ion plasma*, *The Physics of Fluids* **24** (1981) 1447.

[24] G. B. Andresen, M. Ashkezari, M. Baquero-Ruiz, W. Bertsche, P. D. Bowe, E. Butler et al., *Centrifugal separation and equilibration dynamics in an electron-antiproton plasma*, *Physical Review Letters* **106** (2011) 145001.

[25] S. Aghion, C. Amsler, G. Bonomi, R. S. Brusa, M. Caccia, R. Caravita et al., *Compression of a mixed antiproton and electron non-neutral plasma to high densities*, *The European Physical Journal D* **72** (2018) 76.

[26] T. O'Neil, *Cooling of a pure electron plasma by cyclotron radiation*, *The Physics of Fluids* **23** (1980) 725.

[27] A. Povilus, N. DeTal, L. Evans, N. Evetts, J. Fajans, W. Hardy et al., *Electron plasmas cooled by cyclotron-cavity resonance*, *Physical review letters* **117** (2016) 175001.

[28] G. Gabrielse, S. Rolston, L. Haarsma and W. Kells, *Possible antihydrogen production using trapped plasmas*, *Hyperfine Interactions* **44** (1989) 287.

[29] F. Robicheaux, *Atomic processes in antihydrogen experiments: A theoretical and computational perspective*, *Journal of Physics B: Atomic, Molecular and Optical Physics* **41** (2008) 192001.

[30] S. Jonsell, DP. van der Werf, M. Charlton and F. Robicheaux, *Simulation of the formation of antihydrogen in a nested Penning trap: Effect of positron density*, *Journal of Physics B: Atomic, Molecular and Optical Physics* **42** (2009) 215002.

[31] F. Robicheaux, *Simulations of antihydrogen formation*, *Physical Review A* **70** (2004) 022510.

[32] M. E. Glinsky and T. M. O'Neil, *Guiding center atoms: Three-body recombination in a strongly magnetized plasma*, *Physics of Fluids B: Plasma Physics* **3** (1991) 1279.

[33] S. Jonsell and M. Charlton, *On the binding energies of antihydrogen formed by the interactions of antiprotons in cold positron plasmas*, *Journal of Physics B: Atomic, Molecular and Optical Physics* **54** (2021) 025001.

[34] B. Radics, Y. Nagata, Y. Yamazaki, S. Ishikawa, N. Kuroda, Y. Matsuda et al., *The ASACUSA Micromegas Tracker: A cylindrical, bulk Micromegas detector for antimatter research*, *Review of Scientific Instruments* **86** (2015) 083304.

[35] R. G. Greaves, M. D. Tinkle and C. M. Surko, *Creation and uses of positron plasmas*, *Physics of Plasmas* **1** (1994) 1439.

[36] M. Amoretti, C. Amsler, G. Bazzano, G. Bonomi, A. Bouchta, P. D. Bowe et al., *Antihydrogen production temperature dependence*, *Physics Letters B* **583** (2004) 59.

[37] J. R. Danielson, D. H. E. Dubin, R. G. Greaves and C. M. Surko, *Plasma and trap-based techniques for science with positrons*, *Reviews of Modern Physics* **87** (2015) 247.

[38] G. Costantini, L. Giorleo, G. Gosta, M. Leali, V. Mascagna, S. Migliorati et al., *The upgrade of the ASACUSA scintillating bar detector for antiproton annihilation measurements*, *Journal of Instrumentation* **18** (2023) P04013.

[39] N. Kuroda, HA. Torii, M. Shibata, Y. Nagata, D. Barna, M. Hori et al., *Radial compression of an antiproton cloud for production of intense antiproton beams*, *Physical Review Letters* **100** (2008) 203402.

[40] C. F. Driscoll, *Observation of an unstable l=1 diocotron mode on a hollow electron column*, *Physical Review Letters* **64** (1990) 645.

[41] K. S. Fine and C. F. Driscoll, *The finite length diocotron mode*, *Physics of Plasmas* **5** (1998) 601.

[42] M. Amoretti, C. Amsler, G. Bonomi, A. Bouchta, P. Bowe, C. Carraro et al., *Production and detection of cold antihydrogen atoms*, *Nature* **419** (2002) 456.

[43] ATRAP Collaboration, G. Gabrielse, N. S. Bowden, P. Oxley, A. Speck, C. H. Storry et al., *Background-free observation of cold antihydrogen with field-ionization analysis of its states*, *Physical Review Letters* **89** (2002) 213401.

[44] M. Ahmadi, BXR. Alves, CJ. Baker, W. Bertsche, E. Butler, A. Capra et al., *Antihydrogen accumulation for fundamental symmetry tests*, *Nature communications* **8** (2017) 681.